Progress In Electromagnetics Research C, Vol. 21, 179–190, 2011

GAIN ENHANCEMENT OF PLANAR MONOPOLE WITH MAGNETODIELECTRIC MATERIAL

W.-C. Lai †

Department of Electronic Engineering
National Taiwan University of Science and Technology, Taipei, Taiwan

A.-C. Sun

Department of Material Engineering
Yuan Ze University, Jhongli, Taiwan

N.-W. Chen

Department of Communications Engineering
Yuan Ze University, Jhongli, Taiwan

C.-W. Hsue

Department of Electronic Engineering
National Taiwan University of Science and Technology, Taiwan

Abstract—A planar monopole antenna with reconfigurable radiation patterns is demonstrated. The radiation pattern reconfigurability is realized straightforwardly with an employment of a detached magnetodielectric slab placed in the vicinity of the antenna structure. It is shown the radiation patterns can be easily reconfigured through the adjustment of the spacing between the slab and the antenna structure. Technically, the radiated fields are redistributed owing to the inclusion of the magnetodielectric slab, which is of high permittivity, as well as permeability. As a result, the planar monopole gain with the slab is increased up to 4 dBi while the antenna resonant frequency remains almost unchanged.

Received 21 March 2011, Accepted 4 May 2011, Scheduled 10 May 2011
Corresponding author: Ching-Wen Hsue (cwh@mail.ntust.edu.tw).
† Also with Department of Engineering, Ming Chi University of Technology, Taipei, Taiwan.

1. INTRODUCTION

Reconfigurable antennas can be exploited to increase the degrees of freedom and functionality of wireless communication systems. With the antenna's pattern/frequency reconfigurability, the noise sources or intentional interference in a hostile environment are suppressed or alleviated. The antennas of this sort have been reported, e.g., [1–7]. The microelectromechanical systems (MEMS) switched antennas were proposed in [1–3] for reconfigurable radiation-pattern and polarization. Specifically, the MEMS switches integrated with self-similar planar antennas for similar patterns over a wide range of frequencies were demonstrated in [1]. In [2], the MEMS switches are used for radiation pattern reconfigurability of a square spiral microstrip antenna between endfire and broadside over a common impedance bandwidth. Similarly, the antenna design for operation in two different selectable linear polarization bases was proposed in [3]. In [4–7], the PIN diode was employed for the reconfigurable polarization design. For instance, a single-fed microstrip antenna features various polarization diversities was presented in [6]. On the other hand, the single turn square spiral microstrip antenna with both reconfigurable radiation pattern and frequency was demonstrated in [8]. More details on the reconfigurable antenna designs and applications can be found in [9].

Technically, the above-mentioned antenna designs realize pattern/frequency reconfigurability through the modification of the physical configuration of the radiating structure or the incorporation or active devices into the radiating structures. Here, a relatively straightforward approach to realizing reconfigurable radiation patterns is presented. It appears that the antenna radiation characteristics are able to be changed simply with a placement of a detached and thin magnetodielectric slab in the vicinity of the radiating structure [10]. It is shown that the lossy magnetodielectric slab was employed to illustrate the pattern reconfigurabity design for a conventional planar monopole. The slab employment renders the omnidirectional H-plane radiation pattern of the classical monopole directional, and it decreases the radiation efficiency slightly. In addition, the antenna directivity/gain varies drastically with the change of the spacing between the magnetodielectric slab and the radiating element while the antenna operating frequency remains almost unchanged. The radiation pattern reconfigurability is mainly attributed to the high permittivity and permeability of the slab. Technically, the slab essentially redistributes the power flow from the radiating structure and introduces additional phase for the wave passing through it, which synthesize directional radiation patterns.

However, the detailed investigations regarding the impact of the slab placement on antenna characteristics and physical mechanisms of gain enhancement are not provided in [10]. Here, the analysis of the impact of the slab thickness and location on antenna characteristics is presented. Also, the physical mechanisms of the gain enhancement with the slab placement are outlined.

2. RECONFIGURABLE MONOPOLE DESIGN AND ANALYSIS

As depicted in Fig. 1, the entire antenna comprises a main monopole antenna structure and a detached magnetodielectric slab. The monopole length and strip width are denoted as L_{b1} and W_{b1} respectively. The monopole is on a FR4 dielectric substrate of relative permittivity 4.3 and loss tangent 0.022. The length and width of the substrate are denoted as L and W, respectively. The length and width of the microstrip feed line are termed as L_{b2} and W_{b2}, respectively. As for the magnetodielectric slab, the length, width, and thickness are denoted as L_s, W_s, and t, respectively. The relative permittivity, permeability, and loss tangent of the magnetodielectric slab are 60, 20, and 0.2, respectively. The spacing between the monopole and the slab is denoted as d and the antenna structure is characterized with the finite-element-based full-wave electromagnetic solver, HFSS [11].

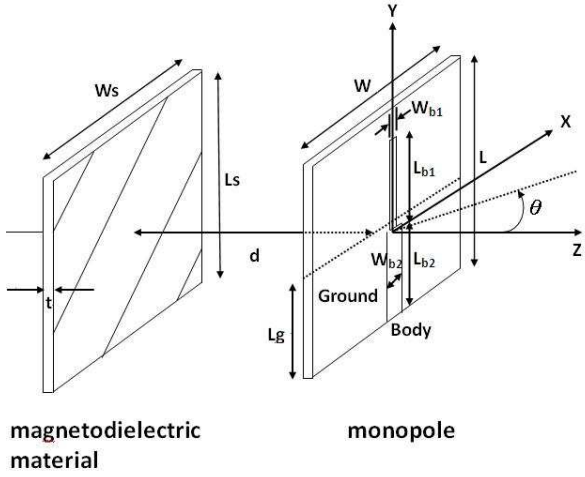

Figure 1. Schematic diagram of the monopole with the magnetodielectric slab.

In what follows, the characterizations on the radiation, return loss, and input impedance are presented in Subsections 2.1, 2.2, and 2.3, respectively. Specifically, Subsection 2.1 demonstrates the antenna near-field redistribution owing to the employment of the magnetodielectric slab. With the near-field redistribution, the variation of the antenna input impedance with respect to different spacing is presented in Subsection 2.2. Finally, the impact of the input impedance variation on the antenna return loss is shown in Subsection 2.3.

2.1. Near Field Redistribution

The antenna with $L = 58.1\,\text{mm}$, $L_g = 30.2\,\text{mm}$, $L_{b1} = 22\,\text{mm}$, $L_{b2} = 21.1\,\text{mm}$, $W = 44.1\,\text{mm}$, $W_{b1} = 1.1\,\text{mm}$, $W_{b2} = 1.9\,\text{mm}$, $L_s = 58.1\,\text{mm}$, $W_s = 44.1\,\text{mm}$, and $t = 1.2\,\text{mm}$ is used to describe the antenna near-field redistribution owing to the employment of the magnetodielectric slab. The dimensions L_{b2} and W_{b2} are chosen for a quarter-wavelength monopole at the resonant frequency 2.4 GHz. On the other hand, the length and width of the FR4 substrate are initially chosen with the rule of the thumb for the traditional printed monopole design. Specifically, the width W is chosen to ensure that the electrical width of the ground plane is greater than half a wavelength at the resonant frequency, and the length L of the substrate is chosen so that fringing fields around the monopole truncated end have no significant impact on the antenna characteristics. The dimensions are optimized with the HFSS. Figs. 2(a), (b), and (c) show the plots of the radiated power flow, i.e., the real part of the complex Poynting vector, of the antenna at the H-plane (xz-plane) at around the resonant frequency (2.3 GHz) for the cases of without the slab, $d = 14\,\text{mm}$ and 36 mm, respectively. Compared to the case without the slab, it is clearly seen that power flow is redistributed/compressed when the magnetic dielectric slab is placed in the vicinity of the monopole antenna. This redistribution is mainly owing to wave-front deformation of the outgoing wave radiated from the monopole. The deformation is attributed to the retarded fields, as well as the field confinement in the slab. Consequently, the near fields and far fields are redistributed with the presence of the slab, which leads to relatively directional radiation patterns.

Specifically, the correlation between slab thickness and the antenna gain is investigated by using a proposed transmission-line equivalent circuit model shown in Fig. 3. The transmission-line circuit model shown in the Fig. 3 is employed to understand the gain enhancement on the slab side, albeit the model is in theoretically not rigorous. In Fig. 3, the slab is modeled as a section of a lossy

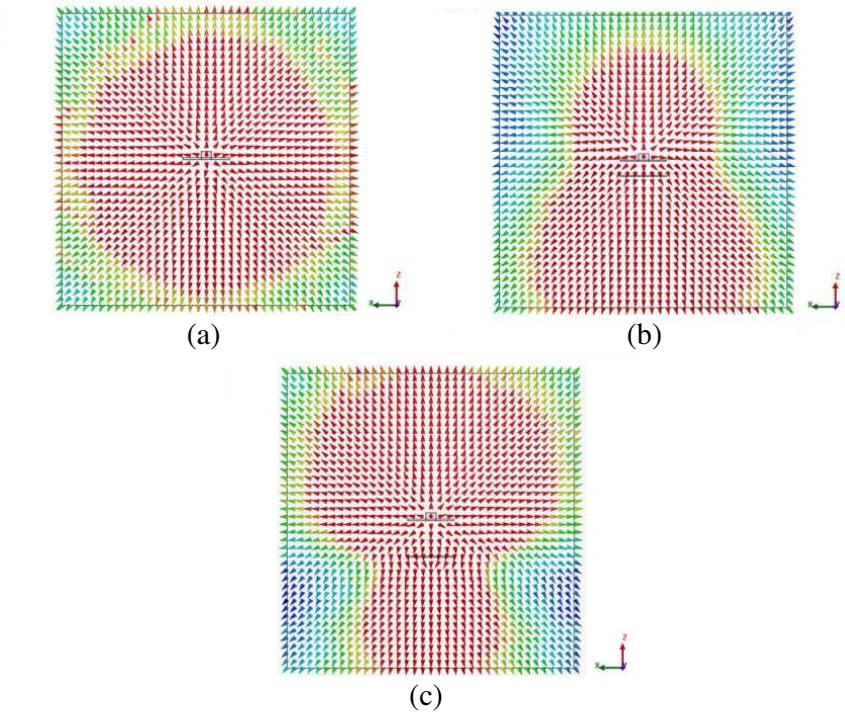

Figure 2. The radiated power plot at the H-plane for the cases (a) without the slab, (b) with the slab and $d = 14\,\text{mm}$, and (c) with the slab and $d = 36\,\text{mm}$. (high intensity: red; low intensity: blue).

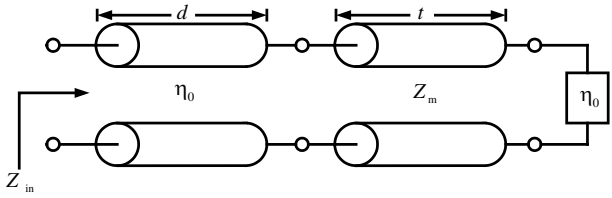

Figure 3. The transmission-line equivalent circuit model for the slab and the free space surrounding the monopole.

transmission line with characteristic impedance Z_m while the air surrounding the slab is modeled as a lossless transmission line with characteristic impedance η_0. Fig. 4 shows the transmitted power through the slab against slab thickness (t) while the spacing d is fixed at 14 mm. Generally speaking, the transmitted power decreases while the

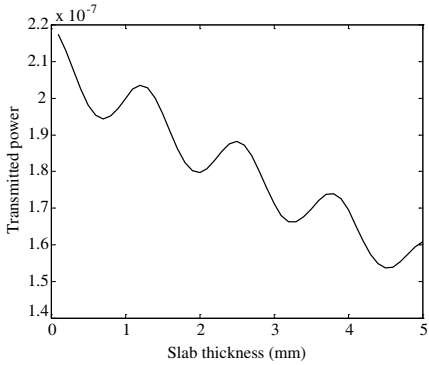

Figure 4. The transmitted power through the slab at different slab thickness.

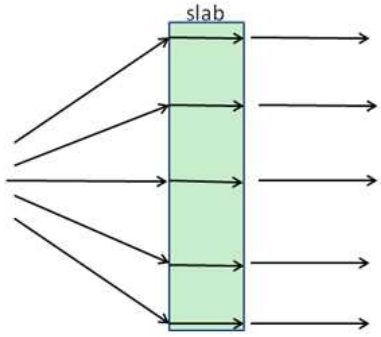

Figure 5. Illustration of the ray trajectories in the vicinity of the slab.

slab thickness increases since the slab is lossy in nature. However, there is a kink at around $t = 1.2\,\text{mm}$, which corresponds to a relatively high transmitted power. On the other hand, the wave experiences a very slow phase velocity in the slab simply due to the high permittivity and permeability of the slab. That is, the slab is of a very high refractive index from the optics point of view. Hence, when the outgoing waves from the monopole impinge the slab, the waves considered as incoming rays toward the slab are bent-see Fig. 5. The aforementioned two physical mechanisms in essence lead to a gain enhancement.

To verify the aforementioned observations, the full-wave analysis using HFSS is employed to characterize the monopole. Fig. 6 shows the antenna gain variation as a function of the slab thickness at different spacing. It is shown that when the slab is placed very close to the monopole antenna structure ($< 6\,\text{mm}$), the near fields are drastically affected by the slab. Specifically, with the slab employment, the enhanced field confinement around the monopole radiating structure together with the relatively high slab loss leads to a significant decrease of the antenna gain. Indeed, the antenna gain drops significantly as the slab is moving toward the monopole. Also, the gain drops as the slab thickness increases. In contrast, the antenna gain becomes greater than the one of the planar monopole when the spacing is larger than 7 mm for the case $t = 1.2\,\text{mm}$ and larger than 10 mm for the cases $t = 0.5\,\text{mm}$ as well as 0.85 mm. Here, the radiated power flow is relatively increased on the slab side mainly owing to the high permittivity and permeability of the slab. On the other hand, the slab leads to additional phase for the wave passing through it. The phase is linearly proportional to the

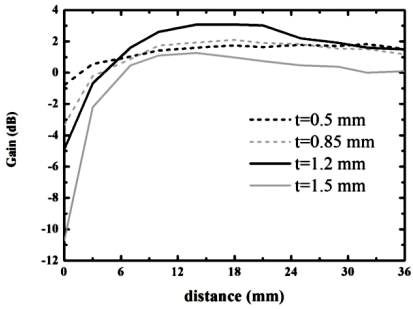

Figure 6. The antenna gain variation as a function of the slab thickness.

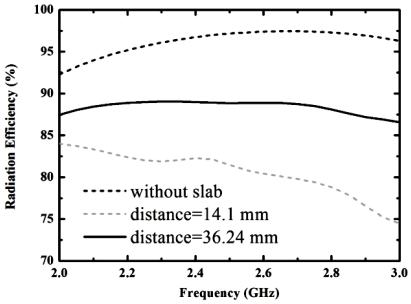

Figure 7. The simulated radiation efficiency of the reconfigurable antenna as a function of the slab thickness.

electrical thickness of the slab. In Fig. 6, it is shown that the case $t = 1.2\,\text{mm}$ has a gain up to 3 dBi, whereas the corresponding gain of the case $t = 1.5\,\text{mm}$ is less than 1 dBi. As a result, the slab thickness is shown to be the other key to the radiation characteristics.

When the slab is placed relatively away from the monopole ($>$ 25 mm), the antenna gain is nearly the same as the one without the slab for the cases $t = 0.5\,\text{mm}$, 0.85 mm, and 1.2 mm. In this case, the impact of the slab on the power flow is relatively minor and the additional loss from the slab essentially results in a smaller gain compared to the one without the slab. Regarding the slab loss, Fig. 7 shows the simulated antenna radiation efficiency with respect to the slab thickness. It is seen that the efficiency is related to the slab thickness as well as the spacing.

2.2. Input Impedance

It is shown that near field of the monopole is redistributed with the employment of the magnetodielectric slab. The near-field redistribution leads to redirection of the power flow. Here, the variation of the antenna input impedance attributed to the near-field redistribution is presented. The simulated input impedance at the frequency 2.4 GHz is tabulated in Table 1. It is shown that the imaginary part of the input impedance increases as the spacing decreases. Again, as the spacing decreases, the reactive energy stored in the region outlined by the monopole and the slab increases, which leads to an increase of the imaginary part of the input impedance. On the other hand, the increase of the real part of the input impedance

Table 1. Simulated input impedance of the reconfigurable monopole.

Without the slab	$d = 7\,\text{mm}$	$d = 14\,\text{mm}$	$d = 32\,\text{mm}$	$d = 36\,\text{mm}$
1.2531 $+0.0050i$	1.4356 $+0.6604i$	1.2910 $+0.6020i$	1.4362 $+0.1862i$	1.4528 $+0.1107i$

increases is attributed to the increase of ohmic loss with the lossy slab employment. Noteworthy, at the spacing $d = 14\,\text{mm}$, the real part of the input impedance slightly increases compared to the case without the slab. That is, with this spacing, the power flow is redirected with minimum loss caused by the slab employment. As a result, the relatively high gain enhancement is observed as shown in Fig. 6.

The abovementioned observations on the antenna input impedance can be explained using the equivalent circuit model shown in Fig. 2. Specifically, the impedance looking into the load at the front of the slab is written as

$$Z_s = Z_m \frac{\eta_0 \cosh(\gamma t) + jZ_m \sinh(\gamma t)}{Z_m \cosh(\gamma t) + j\eta_0 \sinh(\gamma t)} \tag{1}$$

where γ is the wave number in the slab. With Eq. (1), the input impedance Z_{in} can be rewritten as

$$Z_{in} = \eta_0 \frac{Z_s \cos(\beta_0 d) + j\eta_0 \sin(\beta_0 d)}{\eta_0 \cosh(\beta_0 d) + jZ_s \sin(\beta_0 d)} \tag{2}$$

Here, the input impedance against the spacing (d) while the slab thickness is fixed ($t = 1.2\,\text{mm}$) is demonstrated in Fig. 8. It is shown that slab location influences the wave impedance of the outgoing waves from the monopole. Technically speaking, the slab functions like a space impedance transformer. At the spacing ranging from about 12 to 22 mm, the imaginary part of the impedance looking into the transmission-line model shown in Fig. 2 is relatively small while the real part of the impedance is slightly increased. That is, compared to the case without the slab placement, the demonstrated spacing ($d = 14\,\text{mm}$) has a better impedance matching at the antenna feed end, which corresponds a relatively small loss. Meanwhile, the slab directs the outgoing rays and leads to a higher gain.

2.3. Return Loss

In this subsection, the antenna return loss is obtained with the simulated input impedance presented above. It is known the antenna input impedance is related to the antenna near-field

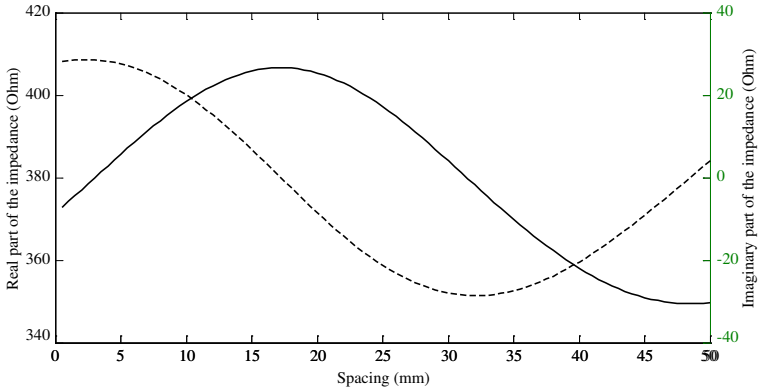

Figure 8. The input impedance of the circuit shown in Fig. 2 at different spacing.

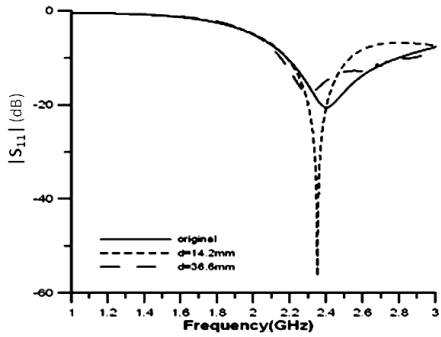

Figure 9. The simulated return loss of the monopole antenna as a function of the spacing.

characteristics [11, 12]. As listed in Table 1, when the slab is placed at the location (around 14 mm) where the resulting gain is higher than the one without its presence, the slab has a minor impact on the resonant frequency as demonstrated in Fig. 9. Again, this is simply owing to that the slab employment slightly changes the real part of the antenna input impedance.

3. EXPERIMENTAL DEMONSTRATION

The photograph of top, side, and bottom views of the fabricated antenna are shown in Figs. 10(a), (b), and (c), respectively. The fabricated monopole dimensions are the same as the simulated one

described in the above section with the slab thickness of $t = 1.2\,\text{mm}$. The measured return loss against different spacing is shown in Fig. 11.

As a result, the antenna resonant frequency remains almost fixed for different thickness. Figs. 12(a) and (b) show the simulated and

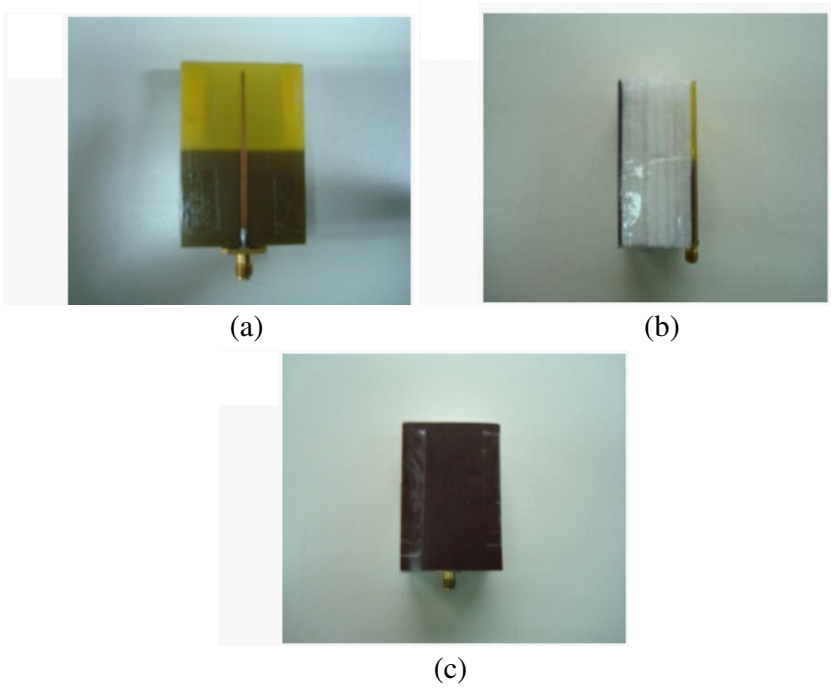

Figure 10. The photographs of the reconfigurable monopole: (a) top view, (b) side view, (c) bottom view.

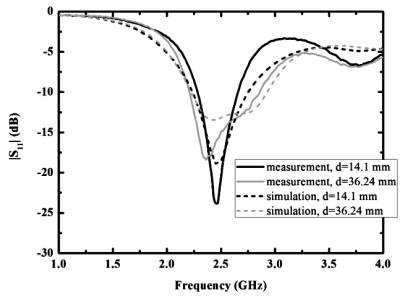

Figure 11. The measured and simulated $|S_{11}|$ of the reconfigurable monopole when $d = 14.1\,\text{mm}$ and $36.24\,\text{mm}$.

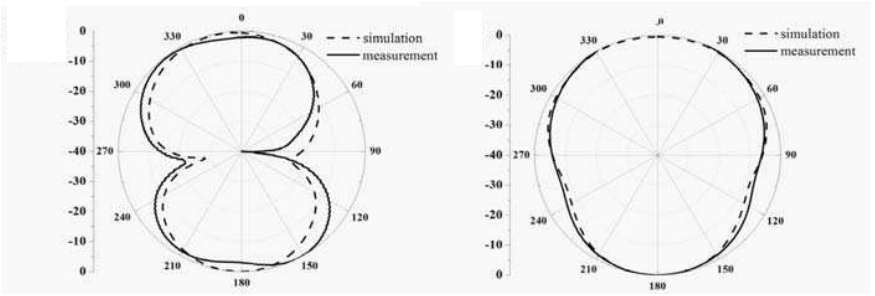

(a) (b)

Figure 12. The measured and simulated radiation patterns of the reconfigurable monopole when $d = 36.24$ mm at (a) E-plane and (b) H-plane.

measured radiation patterns at the E- and H-planes at the resonant frequency (2.3 GHz). It is shown that the measured data are in excellent agreement with the simulated one. Again, in Fig. 12(b), the H-plane radiation pattern becomes directional compared to the one of the classical monopole [13].

4. CONCLUSION AND FUTURE WORK

A planar monopole antenna with reconfigurable radiation pattern is presented. The pattern reconfigurability is achieved with an inclusion of a thin magnetodielectric slab placed around the monopole structure. Owning to the property of high permittivity and permeability, the slab modifies the distribution of the radiated fields from the monopole. Both the slab location and thickness are shown to be the key factors to determine radiation patterns. The reconfigurable monopole with an adjustable gain is demonstrated experimentally for design verification. The demonstrated antenna is expected to find applications in noise or interference suppression for the mobile devices in a hostile environment.

REFERENCES

1. Anagnostou, D., G. Zheng, M. Chryssomallis, J. Lyke, G. Ponchak, J. Papapolymerou, and C. Christodoulou, "Design, fabrication, and measurements of an RF-MEMS-based self-similar reconfigurable antenna," *Proc. Int. Symp. on Circuits and Syst., ISCAS'03*, Vol. 54, 422–432, Feb. 2003.
2. Huff, G. H. and J. T. Bernhard, "Integration of packaged RF

MEMS switches with radiation pattern reconfigurable square spiral microstrip antennas," *IEEE Trans. Antennas Propag.*, Vol. 54, No. 2, 464–469, Feb. 2006.

3. Grau, A., J. Romeu, M.-J. Lee, S. Blanch, L. Jofre, and F. D. Flaviis, "A dual-linearly-polarized MEMS-reconfigurable antenna for narrowband MIMO communication systems," *IEEE Trans. Antennas Propag.*, Vol. 58, No. 1, 4–17, Jan. 2010.
4. Nikolaou, S., R. Bairavasubramanian, C. Lugo, I. Carrasquillo, D. Thompson, G. Ponchak, J. Papapolymerou, and M. Tentzeris, "Pattern and frequency reconfigurable annular slot antenna using PIN diodes," *IEEE Trans. Antennas Propag.*, Vol. 54, No. 2, 439–448, Feb. 2006.
5. Jin, N., F. Yang, and Y. Rahmat-Samii, "A novel reconfigurable patch antenna with both frequency and polarization diversities for wireless communications," *Proc. IEEE Antennas and Propag. Society Int. Symp.*, Vol. 2, 1796–1799, Jun. 2004.
6. Chen, R.-H. and J. S. Row, "Single-fed microstrip patch antenna with switchable polarization," *IEEE Trans. Antennas Propag.*, Vol. 56, No. 4, 922–926, Apr. 2008.
7. Aissat, H., L. Cirio, M. Grzeskowiak, J.-M. Laheurte, and O. Picon, "Reconfigurable circularly polarized antenna for short-range communication systems," *IEEE Trans. Microw. Theory Tech.*, Vol. 54, No. 6, 2856–2863, Jun. 2006.
8. Huff, G. H., J. Feng, S. Zhang, and J. T. Bernhard, "A novel radiation pattern and frequency reconfigurable single turn square microstrip spiral antenna," *IEEE Microw. Wireless Compon. Lett.*, Vol. 13, 57–59, Feb. 2003.
9. Bernhard, J. T., *Reconfigurable Antenna: Synthesis Lectures on Antennas*, Morgan & Claypool, 2007.
10. Lai, W.-C., D.-L. Miao, and C.-W. Hsue, "Effect of magnetic layer on radiation characteristics of monopole antenna," *4th International Conference on Electromagnetic Near-Field Characterization and Imaging (ICONIC 2009)*, 255–258, Taipei, Taiwan, 2009.
11. HFSS 11, Ansoft Corporation (ANSYS) [Online]. Available: www.ansoft.com
12. Pozar, D. M., *Microwave Engineering*, 2nd edition, Wiley, New York, 1998.
13. Balanis, C. A., *Antenna Theory, Analysis and Design*, 2nd edition, Wiley, New York, 1997.